Chinese Chemical Letters 34 (2023) 107416

Contents lists available at ScienceDirect

Chinese Chemical Letters

journal homepage: www.elsevier.com/locate/cclet

One-dimensional ZnSe@N-doped carbon nanofibers with simple electrospinning route for superior Na/K-ion storage

Di Huang[a], Daxiong Wu[b], Jixing Zhu[a], Jinyu Xie[a], Jipeng Wu[a,b], Jiaojiao Liang[a,*]

[a] Hunan University of Technology, Zhuzhou 412008, China
[b] School of Physics and Electronics, Hunan University, Changsha 410082, China

ARTICLE INFO

Article history:
Received 4 January 2022
Revised 6 February 2022
Accepted 7 April 2022
Available online 11 April 2022

Keywords:
ZnSe
Nanofibers
Electrospinning
Na-ion batteries
K-ion batteries
Pseudocapacitive

ABSTRACT

One-dimensional carbon nanofibers are widely applied as anode material in the energy storage field due to its unique structure and high conductivity. In this work, one-dimensional ZnSe@N-doped carbon nanofibers (ZnSe@NC NFs) are successfully synthesized by electrospinning and annealed without extra troublesome conditions. ZnSe nanocrystals are enfolded in the N-doped carbon nanofibers, which can act as a protective layer to avoid the volume expansion of active material and promote ion transport during the cycling process. More importantly, the as-synthesized ZnSe@NC NFs are served as the anode material and display the admirable storage properties for Na/K-ion batteries. The one-dimensional ZnSe@NC NFs material shows the high capacity of 237 mAh/g for Na-ion batteries at a current density of 1 A/g for 2000 cycles. Meanwhile, it also delivers a high discharge capacity of 337 mAh/g for K-ion batteries at 0.2 A/g for 300 cycles. Additionally, it is confirmed that the pseudocapacitive contribution of the nano-structure material is up to 54.5% at a scan rate of 0.6 mV/s through the cyclic voltammetry (CV) measurement in K-ion batteries.

Lithium-ion batteries (Li-ion batteries) have been commercialized in all kinds of portable electronic devices owing to their high power density, long cycling life and high energy density [1,2]. Since the shortages of lithium resource severely impeded the development of large-scale energy storage systems [3–5], sodium ion batteries (Na-ion batteries) and potassium ion batteries (K-ion batteries) are considered as the promising candidates to realize large-scale energy storage due to that of abundant stock of sodium and potassium, and suitable standard redox potential (Na: 2.71 V *vs.* E^0, K: 2.93 V *vs.* E^0) [6–10]. Moreover, anode materials play an important role in the performance of Na/K-ion batteries. However, the radius of Na^+ (1.02 Å) and K^+ (1.38 Å) larger than that of Li^+ (0.76 Å), which seriously hinders the ion diffusion kinetics and greatly limits the insertion/extraction that of into anode material during the charge/discharge process, resulting in inferior electrochemical stability [11–15]. Therefore, Na/K-ion batteries are facing the same challenge to develop high-capacity anode materials. It is desirable to explore suitable anode materials with the big layer spacing and high theoretical capacity, realizing the high specific capacity and long cycle life for the next generation large-scale energy storage systems.

Recently, transitional metal diseleniums (TMDs) including $ReSe_2$ [16], $MoSe_2$ [17], $SnSe_2$ [18], $CoSe_x$ [19,20] and $FeSe_2$ [21,22], *etc.*, have attracted wide attention as potential anode materials for alkali metal ion batteries because of their high theoretical storage capacity and unique physicochemical properties [23]. Zinc selenide (ZnSe) as a member of the TMDs family has obtained extensive interest for Li-ion batteries owing to its environment-friendly, low cost and unique electrochemical reaction mechanism [24–26]. However, like most of anode materials of alloying and conversion reactions, ZnSe suffers from enormous volume expansions leading to the electrode pulverization during the charge/discharge process. In addition, pure ZnSe with low conductivity and inferior ionic diffusion rate will result in the slow dynamic behavior and serious polarization, causing poor cycle life. To solve these issues, a large number of research methods have been applied to improve the electrochemical stability of ZnSe material, including incorporating with mechanically resilient carbon materials [27,28], forming hybrid composites with graphene [29,30] and designing nanostructured ZnSe with hollow structures [31–33]. But there were only several reports of the modified ZnSe for utilizing as the anode material in Na/K-ion batteries compared to other metal selenides, up to now. What is more, one dimensional structure offers high performance in alkali metal ion batteries which is widely applied since it cannot only promote ion transport, but also act as a pro-

* Corresponding author.
E-mail address: liangjiaojiao@hut.edu.cn (J. Liang).

https://doi.org/10.1016/j.cclet.2022.04.014
1001-8417/

tective layer to avoid volume expansion of active material during charge/discharge cycling [1,34].

Therefore, in this report, one-dimensional ZnSe@N-doped carbon nanofibers (ZnSe@NC NFs) have been successfully synthesized with the ordinary condition of directly electrospinning and annealing. The as-synthesized ZnSe@NC NFs material exhibits the higher capacity and better rate capability than ZnO@N-doped carbon nanofibers (ZnO@NC NFs) in the cycling process as the novel anode material for Na/K-ion batteries. As the anode material of Na-ion batteries, the ZnSe@NC NFs obtain the high capacity of 326 mAh/g at a current density of 0.1 A/g for 150 cycles, and the 237 mAh/g at 1 A/g after 2000 cycles. Furthermore, the high discharge capacity of 337 mAh/g is realized at 0.2 A/g for 300 cycles with an ultrahigh capacity retention, and the pseudocapacitive contribution percentage has 54.5% of the total capacity at a scan rate of 0.6 mV/s in K-ion batteries.

The ZnSe@NC NFs material is synthesized with electrospinning and annealed without other additional conditions, and the experimental details are given in Supporting information. And in order to investigate the nano material morphology of ZnSe@NC NFs and ZnO@NC NFs, the SEM and TEM are performed. As shown in Fig. 1a, a relatively uniform nanofiber for ZnSe@NC NFs is gained, which is about 400 nm diameter with rough surface. Moreover, the ZnSe nanoparticles are immobilized on the nanofibers surface at the high resolution SEM image of Fig. 1b, and the low resolution TEM image also further proves it in Fig. 1e. In addition, the high resolution TEM image of ZnSe@NC NFs reveals the clear lattice fringes with interplanar spacing of 0.328 nm, corresponding to the (111) plane of ZnSe, as displayed in Fig. 1f. Furthermore, the illustration of the fourier-transformed crystalline lattice intuitively delivers the interplanar spacing of (111) plane. Figs. 1c and d display the SEM images of ZnO@NC NFs with diffident scale, it is clear that ZnO@NC NFs with about 300 nm diameter and a smooth surface without obvious nanoparticles are observed, which signifies that ZnO is probably wrapped in interior of the carbon nanofibers.

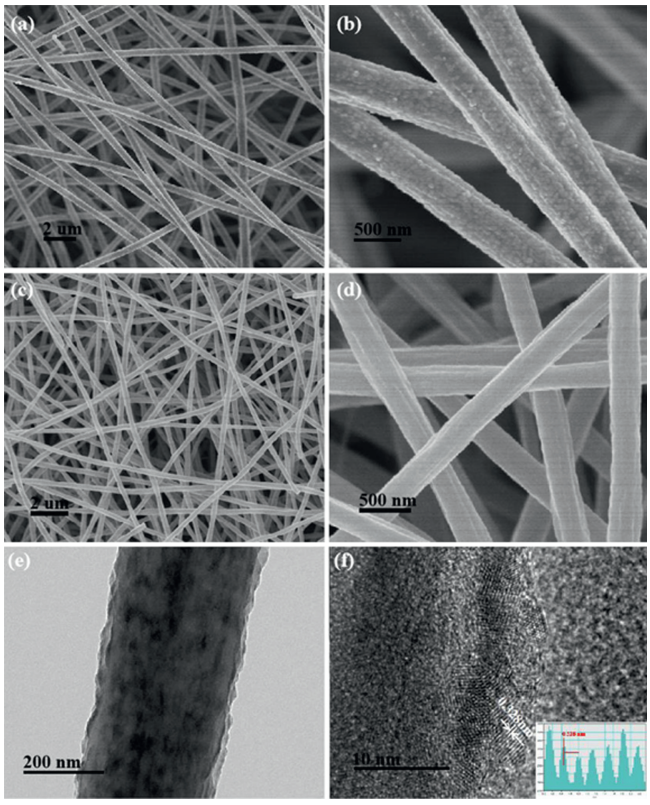

Fig. 1. The SEM images of (a, b) ZnSe@NC NFs and (c, d) ZnO@NC NFs. (e, f) The TEM images of ZnSe@NC NFs.

The detail structure information of the ZnSe@NC NFs and ZnO@NC NFs are further confirmed by X-ray diffraction (XRD) analysis as shown in Fig. S1 (Supporting information). The XRD patterns of ZnO@NC NFs display the relatively weak diffraction peaks at 31.7°, 34.4°, 36.2° and 56.6° corresponding to the lattice planes (100), (002), (101) and (110) of ZnO (PDF standard card No. 74–0534), respectively. These main diffraction peaks are detected in the XRD patterns of ZnSe@NC NFs at 27.2°, 45.2° and 53.5° indexing to the lattice planes (111), (220) and (311) of the cubic ZnSe (PDF standard card No. 37–1463), respectively. In addition, a broad peak appears at around 26.6° corresponding to the lattice planes (111) of C (PDF standard card No. 75–2078). The XRD results indicate that ZnSe@NC NFs and ZnO@NC NFs are successfully synthesized without other intermediate phase. In order to evaluate the contents of ZnSe in ZnSe@NC NFs composites, TGA measurement is characterized in air from room temperature to 700 °C. As displayed in Fig. S2 (Supporting information), a slight weight loss around room temperature to 200 °C corresponding to the volatilization of water. Subsequent weight loss from 200 °C to 500 °C can be illustrated that ZnSe@NC NFs transferred into ZnO, SeO_2 and CO_2. From 500°C to 650°C, SeO_2 is evaporated causing a huge weight loss, and only 25.5% of ZnO remains in the final composites [27,35]. More important thing is that the contents of ZnSe are estimated to be 45.3% from the thermogravimetric curve.

To verify the surface chemical compositions and electronic properties of ZnSe@NC NFs, the X-ray photoelectron spectroscopy (XPS) analyses are carried out. The low-resolution XPS spectra exhibits the main elements of Zn, Se, C and N as displayed in Fig. S3a (Supporting information). The high-resolution XPS spectrum of Zn 2p in Fig. S3b (Supporting information) shows the tow sharp peaks center at binding energies of 1044.6 and 1021.5 eV, which can be indexed to Zn $2p_{1/2}$ and Zn $2p_{3/2}$, respectively. As shown in Fig. S3c (Supporting information), the XPS spectrum of Se 3d is assigned to three peaks of SeO_x, Se $3d_{3/2}$ and Se $3d_{1/2}$ at 58.8, 54.4 and 53.6 eV [33], respectively. The N 1s spectrum is divided into graphitic N, pyrrolic N and pyridinic N at 401.6, 399.8 and 398.2 eV, respectively in Fig. S3d (Supporting information). The presence of N element not only can increases more active sites but also improves the electronic conductivity, leading to the high capacity and excellent rate performance for alkali ion batteries [12].

For exploring the electrochemical properties of ZnSe@NC NFs and ZnO@NC NFs, the ZnSe@NC NFs and ZnO@NC NFs electrodes as the anodes for Na/K-ion batteries are assessed by using electrochemical work station and galvanostatic discharge-charge testing at the voltage range of 0.01–3.0 V. Firstly, the cyclic voltammetry (CV) curves of Na-ion batteries with ZnSe@NC NFs electrode reveals the Na-ion storage behavior *via* recording for the 1st, 2nd, 3rd, 5th and 10th cycles at a scan rate of 0.1 mV/s (Fig. 2a). As expected, a broad reduction peak at ~0.25 V could be related to the intrinsic conversion, the initial Na ion inserting ZnSe and the formation of solid-electrolyte interphase (SEI) in the first cathodic scan [36]. In subsequent scans, the peak weak shifts to the right, indicating an increase of voltage in electrochemical polarization during the sodium reaction in the subsequent cycle [37]. Importantly, the cycles of subsequent scans well overlapped, which demonstrate a good reversibility of the Na-ion storage process for the ZnSe@NC NFs electrode. In addition, two broad oxidation peaks locate at ~0.85 V and ~1.55 V, which could be associated with the two steps of ZnSe regenerated to Zn and Na_2Se in the anodic scan [29]. The charge-discharge profiles at a current density of 0.1 A/g of Na-ion batteries with the ZnSe@NC NFs electrode for 1st, 2nd, 3rd and 5th cycles well correspond to the cathodic/anodic peaks of the CV curves in Fig. 2b.

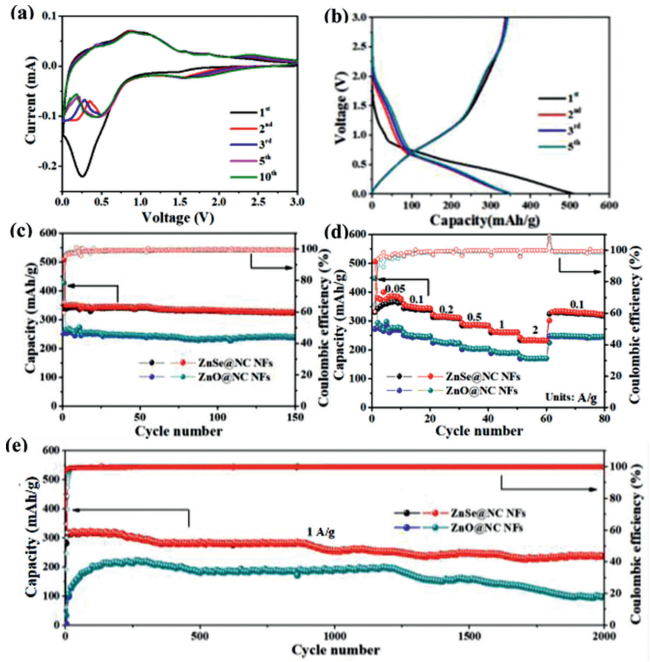

Fig. 2. Electrochemical performance for Na-ion batteries: (a) The CV curve and (b) discharge/charge voltage profile images of the of ZnSe@NC NFs; (c) cycling performances at 0.1 A/g; (d) rate performance and (e) cycling performances at 1 A/g of ZnSe@NC NFs and ZnO@NC NFs .

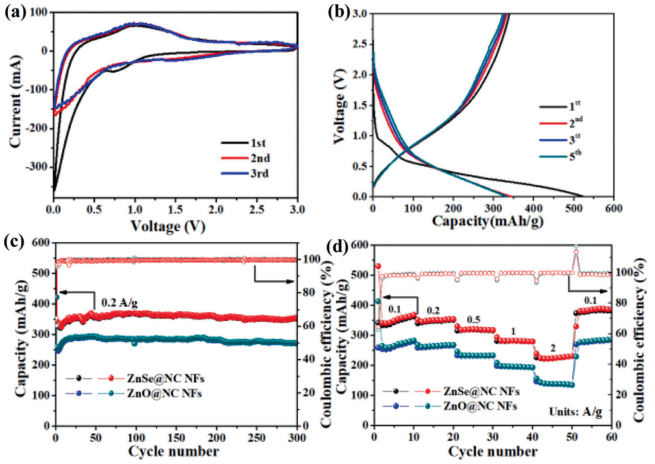

Fig. 3. Electrochemical performance for K-ion batteries: (a) The CV curve and (b) discharge/charge voltage profiles of ZnSe@NC NFs; (c) Cycle performance and (d) rate performance of ZnSe@NC NFs and ZnO@NC NFs electrodes.

The cycling stability of Na-ion batteries with the ZnSe@NC NFs and ZnO@NC NFs are exhibited in Fig. 2c. The ZnSe@NC NFs electrode receives the first discharge/charge capacities capacity of 507.9/336.8 mAh/g at 0.1 A/g in Na-ion batteries, corresponding to the first coulombic efficiency (CE) of 66.3%. The irreversible capacity mainly is owing to forming the SEI on the ZnSe@NC NFs electrode interphase because of the decomposition of solvent molecules in the initial cycle [38]. In the subsequent cycle, the capacity of ZnSe@NC NFs electrode maintains a reversible capacity of 326.4 mAh/g after 150 cycles, and the average CE is over 99.1% throughout the cycle. By contrast, ZnO@NC NFs electrode only obtain the first discharge/charge capacities of 428.1/254.2 mAh/g with a lower first coulombic efficiency (CE) of 59.3% at 0.1 A/g in Na-ion batteries, and the performance is visibly poorer than that of ZnSe@NC NFs electrode. And the rate performance of Na-ion batteries with the two electrodes at various current densities from 0.05 A/g to 2 A/g are displayed in Fig. 2d. Apparently, the performance of Na-ion batteries with ZnSe@NC NFs electrode shows the higher capacity than that with ZnO@NC NFs electrode. More narrowly, it can achieve average reversible capacities of 356.8, 341.1, 312, 284.8 and 260.5 mAh/g at 0.05, 0.1, 0.2, 0.5 and 1A/g, respectively. Even at higher current densities of 2 A/g, the reversible capacities still maintain at 232.9 mAh/g in Na-ion batteries with ZnSe@NC NFs electrode. It is interesting to note that when the current density returns to 0.1 A/g after 60 cycles, the reversible capacities can be rapidly recovered at about 330 mAh/g, indicating the ZnSe@NC NFs as anode of the Na-ion batteries with a good reversibility and fast kinetic behavior. Besides, the long cycle stability of these electrodes at high current density is further investigated in Fig. 2e. The ZnSe@NC NFs electrode gets a high reversible capacity of 237 mAh/g at 1 A/g after 2000 cycles for Na-ion batteries, however, the ZnO@NC NFs electrode only is obtained 96 mAh/g at the same current density in Na-ion batteries.

In addition, the potassium storage of ZnSe@NC NFs and ZnO@NC NFs electrodes is further studied. Firstly, the CV curve for the initial three cycles in the voltage range of 0.01–3 V at a scan rate of 0.2 mV/s are shown in Fig. 3a. In the first cathodic scan, a clear reduction peak appears at ~0.75 V, which could correspond to the conversion/alloying reactions of ZnSe to form ZnK_x and K_2Se, and the formation of the irreversible SEI film on the electrode [32]. For the anodic scan, a weak oxidation peak locates at 1.0 V. It can be indexed to the dealloying reaction of the ZnK_x and oxidation of metallic Zn to ZnSe [39]. In the following scan, the CV curves almost overlap, indicating a good cycling reversibility. What is more, without other distinct oxidation/reduction peaks for K-ion batteries with ZnSe@NC NFs are observed, which might imply that it has the remarkable pseudocapacitance contribution during the charge-discharge processes [40]. Fig. 3b exhibits the charge-discharge voltage profiles at a current density of 0.2 A/g of the ZnSe@NC NFs electrode for 1st, 2nd, 3rd and 5th cycles for K-ion batteries, and the voltage profiles are in accord with the CV curves. Fig. 3c displays the cycling performance of the K-ion batteries with ZnSe@NC NFs and ZnO@NC NFs electrode at 0.2 A/g. The first cycling delivers the discharge/charge capacities of 523.1/339.8 mAh/g at 0.2 A/g with the first CE of 62%, which is better than that with ZnO@NC NFs electrode (421.4/254.3 mAh/g with 60.3% CE). In addition, the ZnSe@NC NFs electrode maintains a highly reversible capacity of 351.6 mAh/g after 300 cycles without capacity decay and ultrahigh average CE of >99.5% in the following cycles, respectively, which reveal an outstanding cycling stability. As shown in Fig. 3d, the K-ion batteries with ZnSe@NC NFs electrode represent the higher specific capacity (346.8, 347.3, 317.8, 280.8 and 225.7 mAh/g) than these with ZnO@NC NFs electrode (265.4, 263.1, 232.4, 195.6 and 139.1 mAh/g) at 0.1, 0.2, 0.5, 1.0 and 2.0 A/g, respectively. What is more, the reversible capacities can be quickly regained to at about 380 mAh/g for the current density returns to 0.1 A/g, demonstrating the relatively excellent rate performance of the ZnSe@NC NFs electrode in K-ion batteries.

In order to further investigate the electrochemical kinetics of the ZnSe@NC NFs electrode in K-ion batteries, the CV measurement is performed at different scan rates from 0.2 mV/s to 2 mV/s in Fig. 4a, and the CV curves are basically the same, while the peak current enhances with the increase of the scan rate, indicating the relatively low polarization of the ZnSe@NC NFs electrode for K-ion batteries [33]. The power-law relationship between the peak current density (i) and scan rate (v) can be described *via* following two equations: $i = av^b$ $(0.5 \le b \le 1)$, $\log(i) = \log(a) + b\log(v)$. The b-value can be obtained by plotting $\log(i)$ *versus* $\log(v)$, and the b-value is close to 0.5, represent-

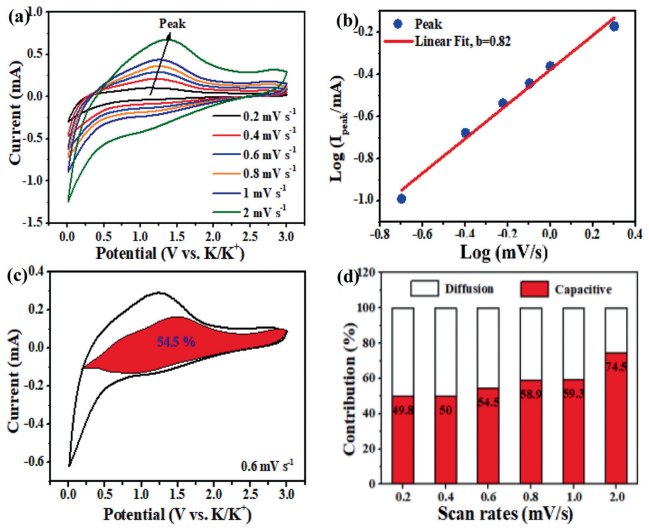

Fig. 4. (a) The CV voltage profilesat different scan rates of 0.2–2.0 mV/s and (b) the plots of log(*i*) *vs.* log(*υ*) of ZnSe@NC NFs in K-ion batteries; (c) the CV profile of capacitive contribution at the scan rate of 0.6 mV/s and (d) the capacitive contribution percentage at different scan rates for K-ion batteries.

ing an ideal diffusion-controlled process, and *b*-value is close to 1.0, demonstrating a capacitive-controlled behavior [41,42]. As revealed in Fig. 4b, the *b*-value of a broad redox position is calculated by linear fitting to be 0.82, implying the contribution of the both capacitive and batteries behaviors for the K-ion batteries with ZnSe@NC NFs electrode. In addition, the capacitive-controlled contribution and diffusion-controlled contribution can be separated to two parts of k_1v and $k_2v^{1/2}$ according to the equation of $i(v)=k_1v+k_2v^{1/2}$. Fig. 4c displays the capacitive-controlled contribution percentages in red regions with 54.5% of the total capacity at a scan rate of 0.6 mV/s. Similarly, the capacitive-controlled contributions of other scan rates have been calculated to 49.8%, 50%, 58.9%, 59.3% and 74.5% corresponding to the scan rates of 0.2, 0.4, 0.8, 1.0 and 2.0 mV/s, respectively (Fig. 4d). These results clearly demonstrate that the ZnSe@NC NFs electrode is co-contribution of the both capacitive and batteries behaviors, rendering that the ZnSe@NC NFs electrodes achieved a remarkable rate performance in K-ion batteries.

In summarize, we have successfully synthesized one-dimensional ZnSe@NC NFs *via* an electrospinning/annealing route without harsh conditions, which the selenium powder is utilized and could be evenly dispersed in the polyacrylonitrile/DMF solution while adding zinc salt. Both one-dimensional nano-structure and N-doping of carbon with ZnSe material contributed to the improvement of the electrochemical performance. And the sodium and potassium storage performance of ZnSe@NC NFs composites are studied and have more prominent storage properties. In addition, the potassium storage kinetics is further explored and the capacitive contribution take possession of more than 50% at high current density. This work can deliver a guidance to explore the composite of TMDs and carbon as the electrode material for Na/K-ion batteries.

Declaration of competing interest

The authors declare that there are no conflicts to declare.

Acknowledgments

This work is supported by the Natural Science Foundation of Hunan Province (Nos. 2020JJ5135 and 2021JJ40168), the Education Department of Hunan Province (Nos. 21B0534 and 20C0602).

Supplementary materials

Supplementary material associated with this article can be found, in the online version, at doi:10.1016/j.cclet.2022.04.014.

References

[1] J. Liang, X. Gao, J. Guo, et al., Sci. Chi. Mater. 61 (2017) 30–38.
[2] D. Wu, C. Wang, M. Wu, et al., J. Energy Chem. 43 (2020) 24–32.
[3] X. Yang, H.J. Liang, H.Y. Yu, et al., J. Phys. Mater. 3 (2020) 042004.
[4] D. Lei, Y.B. He, H. Huang, et al., Nat. Commun. 10 (2019) 4244.
[5] B. Liu, D. Lei, J. Wang, et al., Nano Res. 13 (2020) 2136–2142.
[6] B. Xu, S. Qi, F. Li, et al., Chin. Chem. Lett. 31 (2020) 217–222.
[7] J. Liang, Z. Wei, C. Wang, J. Ma, Electrochim. Acta 285 (2018) 301–308.
[8] G. Qin, Y. Liu, P. Han, et al., Adv. Funct. Mater. 30 (2020) 2005080.
[9] S. Qi, D. Wu, Y. Dong, et al., Chem. Eng. J. 370 (2019) 185–207.
[10] Y.S. Xu, S.J. Guo, X.S. Tao, et al., Adv. Mater. (2021) e2100409.
[11] X. Xie, S. Qi, D. Wu, et al., Chin. Chem. Lett. 31 (2020) 223–226.
[12] D. Wu, W. Zhang, Y. Feng, J. Ma, J. Mater. Chem. A 8 (2020) 2618–2626.
[13] S. Li, W. He, B. Liu, et al., Energy Storage Mater. 25 (2020) 636–643.
[14] X. Rui, X. Zhang, S. Xu, et al., Adv. Funct. Mater. 31 (2020) 2009458.
[15] J. Ge, L. Fan, A.M. Rao, J. Zhou, B. Lu, Nat. Sustain. 5 (2022) 225–234.
[16] X. Xie, M. Mao, S. Qi, J. Ma, CrystEngComm 21 (2019) 3755–3769.
[17] F. Niu, J. Yang, N. Wang, et al., Adv. Funct. Mater. 27 (2017) 1700522.
[18] H. Chen, R. Liu, Y. Wu, et al., Chem. Eng. J. 407 (2020) 126973.
[19] Y. Pan, X. Cheng, M. Gao, et al., ACS Appl. Mater. Interfaces 12 (2020) 33621–33630.
[20] J. Li, D. Yan, T. Lu, Y. Yao, L. Pan, Chem. Eng. J. 325 (2017) 14–24.
[21] M. Yousaf, Z. Wang, Y. Wang, et al., Small 16 (2020) e2002200.
[22] Y. Wu, C. Zhang, H. Zhao, Y. Lei, J. Mater. Chem. A 9 (2021) 9506–9534.
[23] X.X. Jia, X.Z. Yu, B.A. Lu, Rare Metal 40 (2021) 2455–2463.
[24] L. Zhu, Z. Wang, L. Wang, et al., Chem. Eng. J. 364 (2019) 503–513.
[25] H. Liu, Z. Li, L. Zhang, H. Ruan, R. Hu, Nanoscale Res. Lett. 14 (2019) 237.
[26] X. Hu, X. Liu, K. Chen, G. Wang, H. Wang, J. Mater. Chem. A 7 (2019) 11016–11037.
[27] X. Xu, B. Mai, Z. Liu, et al., Chem. Eng. J. 387 (2020) 12406.
[28] C. Tang, X. Wei, X. Cai, et al., ACS Appl. Mater. Interfaces 10 (2018) 19626–19632.
[29] X. Cao, A. Li, Y. Yang, J. Chen, RSC Adv. 8 (2018) 25734–25744.
[30] J. Yuan, W. Liu, X. Zhang, J. Power Sources 455 (2020) 227937.
[31] Y. Zhou, X. Sun, A. Fan, et al., Appl. Surf. Sci. 538 (2021) 148194.
[32] J. Chu, W. Wang, Q. Yu, et al., J. Mater. Chem. A 8 (2020) 779–788.
[33] Y. He, L. Wang, C. Dong, et al., Energy Storage Mater 23 (2019) 35–45.
[34] D. Lei, J. Benson, A. Magasinski, et al., Science 355 (2017) 267–271.
[35] P. Zhou, M. Zhang, L. Wang, et al., Front. Chem. 7 (2019) 569.
[36] S. Lu, T. Zhu, H. Wu, et al., Nano Energy 59 (2019) 762–772.
[37] M. Jia, Y. Jin, C. Zhao, P. Zhao, M. Jia, J. Alloys Compd. 831 (2020) 154749.
[38] X. Li, Z. Han, W. Yang, Adv. Funct. Mater. (2021) 2106194.
[39] C. Dong, L. Wu, Y. He, et al., Small 16 (2020) e2004580.
[40] J. Bai, B. Xi, H. Mao, et al., Adv. Mater. 30 (2018) e1802310.
[41] Z. Liu, T. Lu, T. Song, et al., Energy Environ. Sci. 10 (2017) 1576–1580.
[42] K. Zhang, M. Park, L. Zhou, et al., Adv. Funct. Mater. 26 (2016) 6728–6735.